Journal of Solid State Chemistry 184 (2011) 1661–1665

Contents lists available at ScienceDirect

Journal of Solid State Chemistry

journal homepage: www.elsevier.com/locate/jssc

Oxalic acid mediated synthesis of $WO_3 \cdot H_2O$ nanoplates and self-assembled nanoflowers under mild conditions

Linzhi Li [a], Jingzhe Zhao [a,*], Yi Wang [c,*], Yunling Li [a,b], Dechong Ma [a], Yan Zhao [a,b], Shengnan Hou [a], Xinli Hao [a]

[a] College of Chemistry and Chemical Engineering, Hunan University, Changsha 410082, PR China
[b] College of Chemistry, Jilin University, Changchun, 130012, PR China
[c] Department of Regenerative Medicine, School of Pharmaceutical Sciences, Jilin University, Changchun 130023, PR China

ARTICLE INFO

Article history:
Received 12 February 2011
Received in revised form
26 April 2011
Accepted 2 May 2011
Available online 7 May 2011

Keywords:
$WO_3 \cdot H_2O$
Nanoplate
Nanoflower
Oxalic acid

ABSTRACT

Tungsten oxide hydrate ($WO_3 \cdot H_2O$) nanoplates and flower-like assemblies were successfully synthesized via a simple aqueous method. The effects of reaction parameters in solution on the preparation were studied. Nanoplates and nanoflowers can be selectively prepared by changing the amount of $H_2C_2O_4$. In-situ assembly of nanoplates to nanoflowers was also proposed for the formation of assembled nanostructures. In addition, the reaction time and temperature have important effects on the sizes of the as-obtained samples. Crystal structure, morphology, and composition of final nanostructures were characterized by X-ray diffraction (XRD) and scanning electron microscopy (SEM). Optical properties of the synthesized samples and the growth mechanism were studied by UV–vis detection. Degradation experiments of Rhodamine B (RhB) were also performed on samples of nanoplates and nanoflowers under visible light illumination. Nanoflower sample exhibited preferable photocatalytic property to nanoplate sample.

1. Introduction

Nanomaterials have attracted much attention due to their crucial roles in future technological applications, which are often superior to their corresponding bulk materials [1–5]. It is well-known that physical, optical, and electronic properties of materials are dependent on their shapes with their sizes reduced to micrometer- or nanometer-scales [6]. So, more efforts have been devoted to the synthesis of one-dimensional (1D) nanotubes, nanowires, and nanorods, and two-dimensional (2D) nanoplates and nanodiscs [7–11]. Now, integration of nanorod/nanowire/nanoplate as building blocks into hierarchical superstructures was successfully performed [12–17]. Nanoassembly is an important process for fabrication of functional electronic and photonic nanodevices [18–22]. These novel assembled structures offer opportunities for discovering exciting new properties of materials, and are useful for fabricating complex nanodevices. However, it remains a significant challenge to develop facile, aqueous based, shape controlled and self-assembly routes for the formation of hierarchical nanostructures.

As important wide gap semiconductors, tungsten oxides and tungsten oxide hydrate have many outstanding properties. They have varied applications in many areas, especially gas sensors, field-emission devices, photocatalysts, electrochromic devices, and solar-energy devices [23–27]. Nowadays, a great deal of efforts has been made to prepare 2D tungsten oxides [28–31]. However, these nanostructures are usually produced under high temperatures, long reaction time, and involvement of organic solvents.

For example, He and Zhao [32] successfully synthesized $WO_3 \cdot H_2O$ nanoflakes via a dialysis method with a subsequent aging and drying process, which was aged for 30 days. Chen et al. [29] reported WO_3 nanoplates prepared based on tungstate inorganic–organic hybrid belts conversion. Moreover, although several oxide nanoplates have been reported, there is no example of the assembly of nanoplates into an organized nanostructure under mild conditions. Therefore, preparing nanoplates of tungsten oxides (hydrate) and self-assembled nanoflowers under relative mild conditions still remains a great challenge.

Herein, we report a novel synthesis of $WO_3 \cdot H_2O$ nanocrystals under relative mild conditions. The flower-like assemblies were selectively prepared by adding higher amount of oxalic acid ($H_2C_2O_4$). The structure evolution from plates to flowers was investigated. In this work, $H_2C_2O_4$ is used as a structure-directing agent in the preparation of tungsten oxide (hydrate), and it has

* Corresponding author.
E-mail addresses: zhaojz@hnu.edu.cn, zhao_jingzhe@163.com (J. Zhao).

0022-4596/$ - see front matter © 2011 Elsevier Inc. All rights reserved.
doi:10.1016/j.jssc.2011.05.008

significant effects on the sample formation. Typical nanoplate and nanoflower samples were chosen as photocatalysts for degradation of Rhodamine B (RhB) under visible light illumination. The results showed that nanoflower sample extended preferable photocatalytic property to nanoplate sample.

2. Materials and methods

2.1. Preparation of WO_3 nanoplates

Sodium tungstate ($Na_2WO_4 \cdot 2H_2O$), hydrochloric acid (HCl) and oxalic acid ($H_2C_2O_4$) in A.R. grade were used as purchased in this work without further purification. $Na_2WO_4 \cdot 2H_2O$ was dissolved in 50 mL of deionized water to get a transparent solution of 0.2 M. 50 mL of HCl aqueous solution (2 M) was added dropwise into the above solution under continuous stirring until light yellow precipitates appeared at room temperature, and then the reaction vessel was transferred into a water bath of 90 °C. Certain amount of $H_2C_2O_4$ was subsequently added into the reaction system. After 3 h reaction, the final yellow precipitates were centrifuged and washed repeatedly with deionized water and ethanol, followed by drying them at 60 °C in air, thus $WO_3 \cdot H_2O$ nanoplates or nanoflowers were obtained.

2.2. Powder characterization

The phases of samples were identified by X-ray powder diffraction (XRD), using a Japan D/max-2500 diffractometer with Cu$K\alpha$ ($\lambda = 1.5406$ Å) radiation in a 2θ range from 10° to 80° at room temperature. The morphologies were characterized by scanning electron microscopy (SEM, Hitachi, S-4800). The UV–visible absorption spectra were measured by a Shimadzu UV-1800 pc double-beam UV–visible spectrophotometer.

3. Results and discussions

In our strategy, temperature, reaction time, and $H_2C_2O_4$/Na_2WO_4 ratio have prominent influences on the evolution of $WO_3 \cdot H_2O$ rectangular nanoplates and their assembled nanoflowers. Based on the experimental results, the formation procedure can be described as follows:

$$WO_4^{2-} + 2H^+ + H_2O \rightarrow WO_3 \cdot 2H_2O \quad (1)$$

$$WO_3 \cdot 2H_2O \rightarrow WO_3 \cdot H_2O + H_2O \quad (2)$$

$WO_3 \cdot 2H_2O$ firstly formed as a precursor under acidic condition, and then transformed to $WO_3 \cdot H_2O$ with the help of $H_2C_2O_4$ at mild conditions.

Fig. 1 shows XRD patterns of samples prepared under varied conditions with $H_2C_2O_4$/Na_2WO_4 ratio of 0.25:1. When the system was allowed to react at 90 °C for 3 or 1 h (the samples were signed as W90-3 and W90-1, respectively), the XRD peaks of the samples (Fig. 1a and b) are indexed to orthorhombic tungsten oxide hydrate ($WO_3 \cdot H_2O$, JCPDS No. 84-0886). Paralleled strong and sharp diffraction peaks in the two patterns indicate good crystallinity of the two samples. Compared to sample W90-1, pattern c of the sample prepared at 70 °C for 1 h (signed as W70-1) reveals mixed composition of $WO_3 \cdot 2H_2O$ and $WO_3 \cdot H_2O$. Herein, $H_2C_2O_4$ is a structure-directing agent, the transformation from $WO_3 \cdot 2H_2O$ to $WO_3 \cdot H_2O$ could not occur without its introduction. The result of Fig. 1c indicates slower transformation from $WO_3 \cdot 2H_2O$ to $WO_3 \cdot H_2O$ at lower temperatures and weaker crystallization of $WO_3 \cdot H_2O$ is the result.

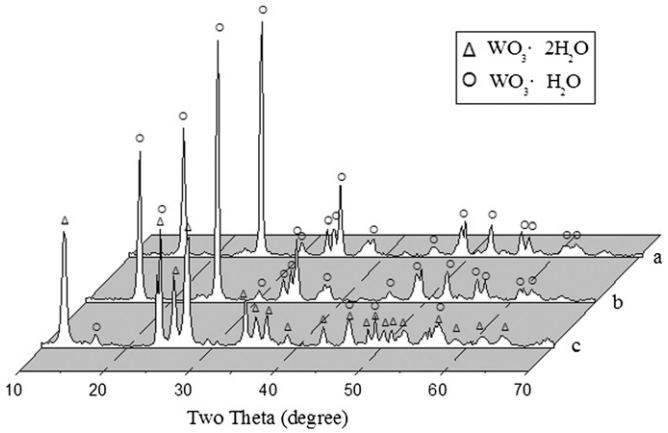

Fig. 1. XRD patterns of W90-3 (a), W90-1 (b), and W70-1 (c) samples prepared at 90 °C for 3 h, 90 °C for 1 h, and 70 °C for 1 h with an $H_2C_2O_4$ to Na_2WO_4 ratio of 0.25:1.

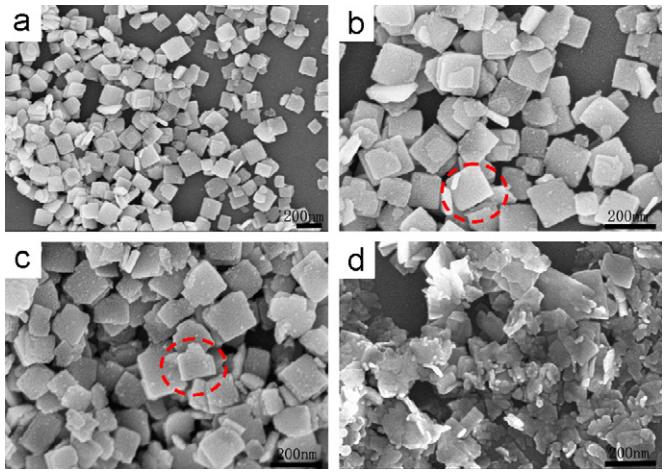

Fig. 2. FESEM images of W90-3 (a, b), W90-1 (c), and W70-1 (d) samples prepared at varied temperature and reaction time with a $H_2C_2O_4$ to Na_2WO_4 ratio of 0.25:1.

The morphologies of the three samples (W90-3, W90-1, and W70-1) were detected by HRSEM, and the results are given in Fig. 2. W90-3 sample extends perfect square plate-like structure in Fig. 2a and b with uniform size and good dispersibility. Closer examination of Fig. 2b shows that the nanoplates have an average size of 150 nm with a thickness of about 25 nm; smooth surfaces and edges with sharp corners are the case in most of the nanoplates. Sample W90-1 in Fig. 2c also has a similar morphology as sample W90-3; however the difference between the two samples is that nanoplates in sample W90-1 appeared as rough surfaces and non-integrated edges, revealing their less crystallization status. Sample W70-1 of lower temperature exhibits only irregular sheet-like segments (Fig. 2d). Based on the results and analyses, we choose W90-3 as the representative sample of $WO_3 \cdot H_2O$ nanoplates in our strategy.

Further experiments were also performed at lower temperature of 70 °C by prolonging the reaction time to 3 h. The sample was signed as W70-3, from the FESEM images in Fig. 3; we can see that rectangular plate-like nanostructures prevail in the sample instead of irregular sheets of sample W70-1; the morphology is similar with that of sample W90-1. This describes that, to achieve similar morphology and crystallization status of the samples, longer reaction time must be consumed at lower temperatures. The mean size of sample W70-3 is decreased to 110 nm compared with 150 nm sized sample W90-3. Combining

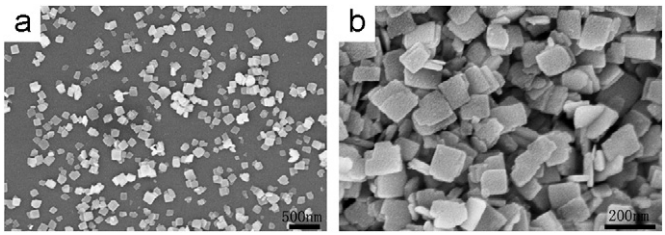

Fig. 3. FESEM images of sample W70-3 with low (a) and high (b) magnifications ($H_2C_2O_4$:Na_2WO_4=0.25:1).

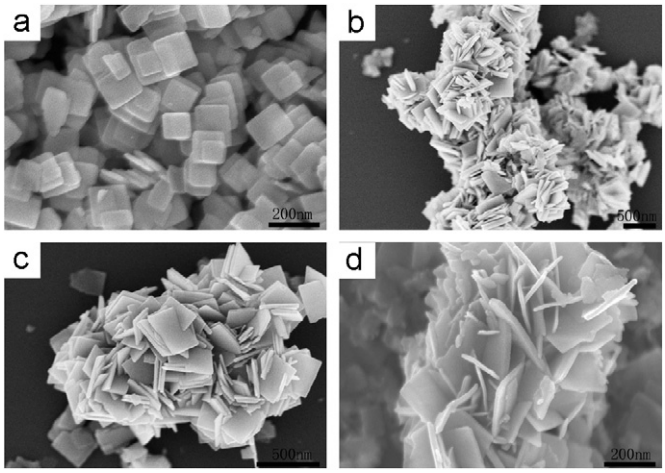

Fig. 4. FESEM images of the samples prepared at varied temperature, time, and $H_2C_2O_4/Na_2WO_4$ ratio. (a) 90 °C–3 h, $H_2C_2O_4/Na_2WO_4$=1:1; (b) 90 °C–3 h, $H_2C_2O_4/Na_2WO_4$=1.5:1; (c) 90 °C–1 h, $H_2C_2O_4/Na_2WO_4$=1.5:1; and (d) 70 °C–1 h, $H_2C_2O_4/Na_2WO_4$=1.5:1.

with the results of Figs. 2 and 3, a conclusion can be made that crystallization and shape evolvement of the square nanoplates can be evaluated at higher temperature or longer reaction time. It also can be seen from the FESEM images of sample W70-3 that coupled nanoplates exist in more places than that of sample W90-3.

In the experiments, we found that the introduction amount of $H_2C_2O_4$ played an important role on determining the crystal growth and the particle assembly styles. In the representative experiment of single-dispersed nanoplates, the molar ratio of $H_2C_2O_4$ to Na_2WO_4 is 0.25:1, with reaction temperature of 90 °C and time of 3 h. As $H_2C_2O_4/Na_2WO_4$ ratio reached 1:1 by increasing the $H_2C_2O_4$ amount, rectangular nanoplates started to aggregate face to face, and more stacked nanoplates emerged in the sample, as shown in Fig. 4a. The size of nanoplates has a slighter change compared to sample W90-3 ($H_2C_2O_4/Na_2WO_4$=0.25:1); the average length of plates is 125 nm with size distribution from 100 to 160 nm. It is the adsorption of more $H_2C_2O_4$ on nanoplates that affected the growth of crystals. When $H_2C_2O_4/Na_2WO_4$ ratio increased to 1.5:1 with other reaction parameters unchanged, the morphology and the aggregation style of the sample changed distinctively. SEM image in Fig. 4b clearly shows that numerous nanoplates were organized into hierarchical structures of nanoflowers, the platelets stacked together in a way of oblique cutting. We also found similar flower-like assemblies in the samples prepared at varied temperature or/and changed reaction time with the same $H_2C_2O_4/Na_2WO_4$ ratio of 1.5:1. Fig. 4c and d gives the assembled nanoflowers of two samples prepared at 90 °C–1 h and 70 °C–1 h, respectively. All the three samples (Figs. 4b–d) appeared as nanoplate-constructed assemblies. The differences of the nanoflowers are the variation in size and thickness of the nanoplates. This reveals that more introduction of $H_2C_2O_4$ results in the formation of self-assembled nanoflowers. To conclude, the amount of oxalic acid plays a key role in the size of nanoplates and their assembly style.

UV–vis detection was also done on the samples with varied amounts of $H_2C_2O_4$ (prepared at 90 °C–3 h); the results are shown in Fig. 5. Detection result of commercial $H_2C_2O_4$ is also given in Fig. 5 for comparison, which is dominated by a prominent peak at 225 nm. In Fig. 5, curve a presents the optical property of the typical nanoplate sample with $H_2C_2O_4/Na_2WO_4$ ratio of 0.25:1 (sample W90-3). There are two narrow peaks centered at 235 and 360 nm; they are reasonably corresponding to absorbance of $H_2C_2O_4$ and $WO_3 \cdot H_2O$, respectively. For curves b–e with an increase in $H_2C_2O_4/Na_2WO_4$ ratio, obvious red-shift of the two peaks occurs compared to curve a. The red-shifts of the peaks reveal the strong interaction between $H_2C_2O_4$ and $WO_3 \cdot H_2O$ in the samples. This further gives us interpretation why $H_2C_2O_4$ plays a key role in our preparation. The nanoflower sample with $H_2C_2O_4/Na_2WO_4$ ratio of 1.5:1 (curve e) has the largest red-shift of the absorbance peaks; it demonstrates the strongest effect of $H_2C_2O_4$ in the sample. In addition, we can also find from the curves that samples with more $H_2C_2O_4$ introduction exhibit broader peaks relative to typical nanoplate sample. This phenomenon was formally reported in literatures as the assembly of single particles [33], and in our case stacked nanoplates or nanoflowers in samples resulted in the broad aspect and red-shift of peaks.

Further experiments give us information that no or less introduction of $H_2C_2O_4$ to the representative reaction system results in irregular nanoparticles and large spherical aggregates instead of rectangular nanoplates or nanoflowers in the samples. The morphologies of the two chosen samples are shown in Fig. 6.

In the typical syntheses, certain amount of oxalic acid is essential to determine the evolution of tungsten oxide hydrate crystals and assembled nanostructures. UV–vis absorption spectroscopy was performed on spherical-like sample with no $H_2C_2O_4$ introduction, and no absorbance peaks relative to $WO_3 \cdot H_2O$ was found in the curve, it only showed the characteristic of $WO_3 \cdot 2H_2O$. This means the spherical aggregates in Fig. 6a are $WO_3 \cdot 2H_2O$, and the transformation to $WO_3 \cdot H_2O$ could occur with the existence of $H_2C_2O_4$ in our strategy.

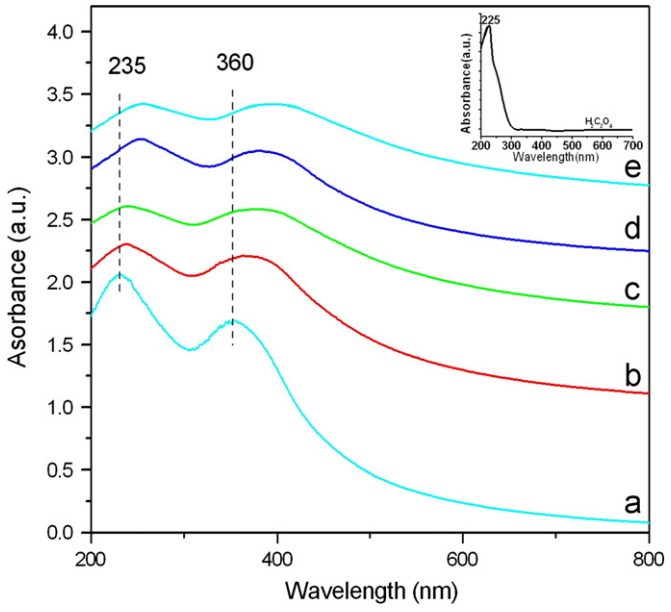

Fig. 5. UV–vis absorption spectra of $WO_3 \cdot H_2O$ samples with $H_2C_2O_4/Na_2WO_4$ ratio of 0.25:1 (a), 0.5:1 (b), 1:1 (c), 1.25:1 (d), and 1.5:1 (e).

It is well known that $WO_3 \cdot 2H_2O$ are built from layers of corner-sharing $WO_5(OH_2)$ octahedra and interlayer water, the schematic structure of which is shown in Fig. 7a. $WO_5(OH_2)$ octahedra consists of four W–O bonds, one W═O bond, and one W–OH_2 (structural H_2O) [32]. The interlayer water connects with $WO_5(OH_2)$ octahedra through hydrogen bonds. Thus $WO_3 \cdot H_2O$ (Fig. 7b) can be obtained through the removal of interlayer water from $WO_3 \cdot 2H_2O$ [34]. The process is illustrated from Fig. 7a and b, which reveals that hydrogen bonds between the interlayer water and structural water were destroyed with the help of $H_2C_2O_4$. In our aqueous experiments, $H_2C_2O_4$ played a key role in the dehydration process at low temperatures (70–90 °C). If no or less $H_2C_2O_4$ was introduced into the representative reaction system, pure $WO_3 \cdot H_2O$ could not generate. $H_2C_2O_4$ is an electron-rich organic molecule involving four O atoms; for this case, one $C_2O_4^{2-}$ ion in aqueous solution can form hydrogen bonds with four different interlayer H_2O molecules in $WO_3 \cdot 2H_2O$, as schemed in Fig. 7c. The strong interactions of $C_2O_4^{2-}$ with interlayer water destroyed the hydrogen bonds between interlayer water and $WO_5(OH_2)$ octahedra, thus speeding up the dehydration process of $WO_3 \cdot 2H_2O$ to $WO_3 \cdot H_2O$. This dehydration mechanism is coincided with our experimental phenomena.

From our experimental results, we knew that the variation of $H_2C_2O_4$ amount in the reaction system not only influenced the crystal structure of samples, but also determined their growth style. Combined with the mechanism analyzed above, a conclusion can be made that when the introduction of $H_2C_2O_4$ was less as $H_2C_2O_4/Na_2WO_4$ ratio of 0.25:1, $H_2C_2O_4$ mainly controlled the dehydration process, thus nanoplates being formed in the samples. If the introduction of $H_2C_2O_4$ increased to enough amount (such as $H_2C_2O_4/Na_2WO_4$ ratio of 1.5:1 in our strategy), $C_2O_4^{2-}$ ions in the reaction system would further form hydrogen bonds with structural water of $WO_5(OH_2)$ (i.e. $WO_3 \cdot H_2O$), which made nanoplates join together, and eventually resulted in the aggregation of nanoplates, hence the samples appeared in a flower-like morphology.

The typical nanoplates (W90-3) and nanoflowers (the sample of Fig. 4b) were also chosen as photocatalysts for degradation of Rhodamine B (RhB) under visible-light stimulation. The photoreactor was composed of a 100 mL beaker and a tungsten filament lamp of 100 W ($\lambda > 400$ nm). A known mass of RhB was dissolved in 100 mL of deionized water to get RhB solution (2 mg/L) in the beaker, and then 0.06 g of $WO_3 \cdot H_2O$ was added into the above solution. The distance from light source to suspension surface was 8 cm, the suspension was kept stirring in the whole photocatalytic experiment, and the system was open to air. Prior to illumination, the suspension was magnetically stirred in darkness for 60 min so as to reach adsorption–desorption equilibrium between RhB molecules and $WO_3 \cdot H_2O$ catalysts.

After that, the solution was irradiated by simulated visible-light. Approximately 2 mL of suspension was taken out from the beaker at certain intervals, and centrifuged to obtain RhB solution. The concentration of RhB in the solution was analyzed by a Shimadzu UV-1800 spectrophotometer. The maximum absorption (λ_{max}) for RhB is 553 nm. Based on analyzing the intensity changes of 553 nm peak during the degradation process, degradation rates of different stages were obtained, which were plotted versus reaction time in Fig. 8.

It can been seen from Fig. 8 that two kinds of suspensions (nanoplates and nanoflowers) reached adsorption–desorption equilibrium 40 min later, but the adsorption rate of nanoflower sample was slightly higher than that of the nanoplate sample. At the time of 60 min, simulated visible-light was on, and degradation reaction of RhB began. In the time range of 60–180 min, the RhB degradation rate of two samples increased slowly. However, the degradation rate of nanoflowers significantly improved at 180 min later; it reached 41.3% at 240 min, while the nanoplate sample still kept a degradation rate of 16%. The preferable photocatalytic activity of nanoflower sample compared to nanoplates should owe to its intense absorption in visible light wavelengths; from Fig. 5 we can see the absorption peak of $WO_3 \cdot H_2O$ in nanoflower sample locates around 402 nm, which convinces the degradation result.

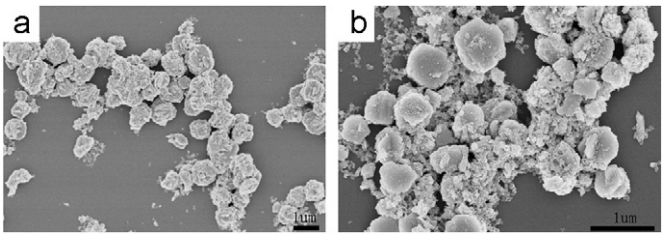

Fig. 6. FESEM images of the samples prepared at 90 °C–3 h with no (a) and less (b) introduction of oxalic acid to the reaction system. For the sample of figure b, the molar ratio of $H_2C_2O_4/Na_2WO_4$ is 0.025:1.

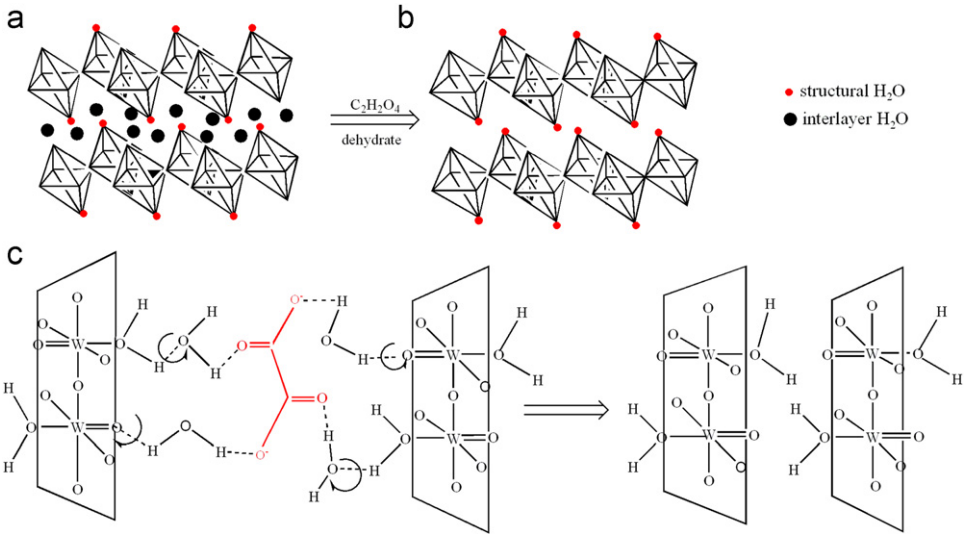

Fig. 7. Structures of (a) layered $WO_3 \cdot 2H_2O$ and (b) $WO_3 \cdot H_2O$ prepared from $WO_3 \cdot 2H_2O$, and (c) the role of oxalic acid with respect to the dehydration process of $WO_3 \cdot 2H_2O$ to $WO_3 \cdot H_2O$.

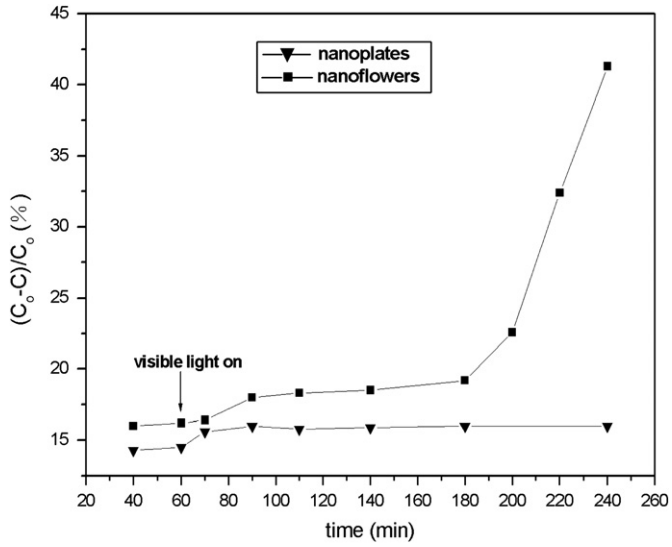

Fig. 8. Visible-light induced degradation of RhB with two typical samples (nanoplates and nanoflowers) as photocatalysts.

4. Conclusion

In summary, tungsten oxide hydrate nanoplates and nanoflowers were synthesized successfully with induction of oxalic acid under mild conditions. $H_2C_2O_4$ played an important role in the evolvement of $WO_3 \cdot H_2O$ crystals and its assembly to flower-like structures. Manipulating the molar ratio of $H_2C_2O_4/Na_2WO_4$, $WO_3 \cdot H_2O$ crystals can be controlled to be isolated rectangular nanoplates, coupled nanoplates, and plate-assembled nanoflowers. The size of the elementary nanoplates is estimated to be 100–160 nm. The possible evolution mechanism was investigated combining FESEM and UV–vis methods. Red-shift of UV–vis absorbance peaks in $H_2C_2O_4$ mediated $WO_3 \cdot H_2O$ samples conceals strong interactions between $H_2C_2O_4$ and $WO_3 \cdot H_2O$. In this paper, we report a one-step approach in the formation of interesting assembled nanostructure, which is worth learning in the synthesis of other substances. Typical nanoplate and nanoflower samples were used as photocatalysts for RhB degradation under simulated visible light. The degradation experiments revealed preferable photocatalytic property of nanoflowers compared to nanoplates.

Acknowledgments

This work was supported by the National Program on Key Basic Research Project (973 Program) (Grant no. 2007CB310503), the Science and Technology Project of Changsha City (Grant no. k0905033-11), and also by the National Natural Science Foundation of China (Grant no. J0830415).

References

[1] X.G. Peng, L. Manna, W.D. Yang, J. Wikham, E. Scher, A. Kadavanich, A.P. Alivisatos, Nature 404 (2000) 59–61.
[2] J.S. Xie, Q.S. Wu, D. Zhang, Y.P. Ding, Cryst. Growth Des. 9 (2009) 3889–3897.
[3] J. Chen, F.Y. Cheng, Acc. Chem. Res 42 (2009) 713–723.
[4] N. Tian, Z.Y. Zhou, S.G. Sun, J. Phys. Chem. C 112 (2008) 19801–19817.
[5] M.H. Huang, S. Mao, H. Feick, H.Q. Yan, Y.Y. Wu, H. Kind, E. Weber, R. Russo, P.D. Yang, Science 292 (2001) 1897–1899.
[6] J. Polleux, A. Gurlo, N. Barsan, U. Weimar, M. Antonietti, M. Niederberger, Angew. Chem. Int. Ed. 45 (2006) 261–265.
[7] Z.X. Wang, S.X. Zhou, L.M. Wu, Adv. Funct. Mater. 17 (2007) 1790–1794.
[8] X.Y. Yang, G.M. Wang, P. Slattery, J.Z. Zhang, Y. Li, Cryst. Growth Des. 10 (2010) 2479–2482.
[9] D. Seo, H.J. Song, J. Am. Chem. Soc. 131 (2009) 18210–18211.
[10] S.G. Yang, Y.P. Wang, Q.F. Wang, R.L. Zhang, Z.M. Yang, Y. Guo, Cryst. Growth Des. 7 (2007) 2258–2261.
[11] J. Samson, A. Varotto, P.C. Nahirney, A. Toschi, I. Piscopo, C. Michael Drain, ACS Nano 3 (2009) 339–344.
[12] X.F. Song, L. Gao, J. Phys. Chem. C 112 (2008) 15299–15305.
[13] J.Z. Yin, Q.Y. Lu, Z.N. Yu, J.J. Wang, H. Pang, F. Gao, Cryst. Growth Des. 10 (2010) 40–43.
[14] Z.J. Gu, T.Y. Zhai, B.F. Gao, X.H. Sheng, Y.B. Wang, H.B. Fu, Y. Ma, J.N. Yao, J. Phys. Chem. B 110 (2006) 23829–23836.
[15] W.S. Wang, L. Zhen, C.Y. Xu, L. Yang, W.Z. Shao, Cryst. Growth Des. 8 (2008) 1734–1740.
[16] G.Z. Shen, Y. Bando, C.J. Lee, J. Phys. Chem. B 109 (2005) 10578.
[17] D.K. Ma, S.M. Huang, W.X. Chen, S.W. Hu, F.F. Shi, K.I. Fan, J. Phys. Chem. C 113 (2009) 4369–4374.
[18] Z.G. An, J.J. Zhang, S.L. Pan, F. Yu, J. Phys. Chem. C 113 (2009) 8092–8096.
[19] Y. Cai, C.M. Lieber, Science 291 (2001) 851.
[20] J. Wu, F. Duan, Y. Zheng, Yi. Xie, J. Phys. Chem. C 111 (2007) 12866–12871.
[21] C.H. Wang, C.L. Shao, Y.C. Liu, X.H. Li, Inorg. Chem. 48 (2009) 1105–1113.
[22] N. Leng, L.Z. Gao, P. Feng, J.Y. Zhang, X.Q. Fu, Y.G. Liu, X.Y. Yan, T.H. Wang, Small 2 (2006) 621.
[23] X.L. Li, T.J. Lou, X.M. Sun, Y.D. Li, Inorg. Chem. 43 (2004) 5442–5449.
[24] J. Zhou, L. Gong, S.Z. Deng, J. Chen, J.C. She, N.S. Xu, R.S. Yang, Z.L. Wang, Appl. Phys. Lett. 87 (2005) 223108.
[25] S. Baeck, K. Choi, T.F. Jaramillo, G.D. Stucky, E.W. McFarland, Adv. Mater. 15 (2003) 1269–1273.
[26] C. Santato, M. Odziemkowshi, M. Ulmann, J. Augustynski, J. Am. Chem. Soc. 123 (2001) 10639–10649.
[27] S. Pokhrel, C.E. Simion, V.S. Teodorescu, N. Barsan, U. Weimar, Adv. Funct. Mater. 19 (2009) 1767–1774.
[28] A. Wolcott, T.R. Kuykendall, W. Chen, S.W. Chen, J.Z. Zhang, J. Phys. Chem. B 110 (2006) 2528–25296.
[29] D.L. Chen, L. Gao, A. Yasumori, K. Kuroda, Y. Sugahara, Small 4 (2008) 1813–1822.
[30] J. Polleux, N. Pinna, M. Antonietti, M. Niederberger, J. Am. Chem. Soc. 127 (2005) 15595–15601.
[31] J.M. Wang, P.S. Lee, J. Ma, J. Cryst. Growth 311 (2009) 316–319.
[32] Y.P. He, Y.P. Zhao, J. Phys. Chem. C 112 (2008) 61–68.
[33] T.S. Sreeprasad, A.K. Samal, T. Pradeep, Langmuir 24 (2008) 4589–4599.
[34] Y.M. Li, M. Hibino, M. Miyayania, T. Kudo, Solid State Ionics 134 (2000) 271.